FINAL TECHNICAL REPORT

Structure and Dynamics of the Coronal Magnetic Field

NASA Space Physics Theory Grant NAG5-2257

(5/1/93 to 4/30/96)

submitted

by

Gerard Van Hoven, Principal Investigator

Department of Physics and Astronomy

University of California

Irvine, CA 92697-4575

and

Dalton D. Schnack, Senior Scientist

Applied Physics Operation

Science Applications International Corporation

10260 Campus Point Drive

San Diego, CA 92121

July 31, 1996

Table of Contents

FINAL TECHNICAL REPORT

The NASA Space-Physics-Theory program, "Structure and Dynamics of the Coronal Magnetic Field," has been supported by Grant NAG5-2257 at the University of California, Irvine, and Science Applications International Corporation, San Diego, since 1 May 1993. During this period, the UCI/SAIC group has produced 25 refereed publications [listed in the Appendix] and one Ph.D. dissertation acknowledging this grant. The results of this research effort have been described in a number of Invited Papers presented at scientific meetings and workshops.

1. INTRODUCTION

One of the fundamental problems of solar-terrestrial physics is to understand the relationship between solar and geomagnetic activity, a connection that was first noted more than a century ago by Carrington (1860). Geomagnetic activity can have adverse consequences for our society as we become more dependent on advanced technology. Apart from the pure intellectual attraction that we have for understanding the complex phenomena observed on our nearest star, the Sun, it is the obligation of solar physicists to develop a quantitative understanding of, and eventually a predictive capability for, solar eruptions, since the Sun is the driver of terrestrial geomagnetic disturbances. This Sun-Earth connection, dubbed "space-weather," has recently been recognized as an important activity for the space-science community.

The last few years have seen a marked increase in the sophistication of models of the solar corona. This has been brought about by a confluence of three key elements. First, the collection of high-resolution observations of the Sun, both in space and time, has grown tremendously (e.g., Yohkoh images of the X-ray Sun, Ulysses measurements of the polar solar wind, high-resolution white-light movies of solar granulation, and high-resolution vector magnetographs of active regions). The SOHO (Solar Heliospheric Observatory) mission is providing additional correlated high-resolution magnetic, white-light and spectroscopic observations. Second, the power and availability of supercomputers has made two- and three-dimensional modeling routine. Third, the sophistication of the models themselves, both in their geometrical realism and in the detailed physics that has been included, has improved significantly.

The support from our current Space Physics Theory grant has allowed us to exploit this confluence of capabilities. We have carried out direct comparisons between observations and models of the solar corona. The agreement between simulated coronal structure and observations has verified that the models are mature enough for detailed analysis, as we will describe. The development of this capability is especially timely, since observations obtained from three space missions that are under way (Ulysses, WIND and SOHO) offer an opportunity for significant advances in our understanding of the corona and heliosphere. Through this interplay of observations and theory we can improve our understanding of the Sun.

2. ACHIEVEMENTS

In this section we summarize the accomplishments made by the UCI/SAIC group during the current Space Physics Theory Program grant. The descriptions are necessarily brief, and are

primarily intended to illustrate the breadth and principal results of the research we have undertaken. A full account can be found in the publications listed in the Appendix.

2.1. Modeling the Large-Scale Structure of the Solar Corona

The interaction of the solar wind with coronal magnetic fields produces the beautiful helmet streamers that can be seen during solar eclipses. Coronal streamers are dense structures that form in regions where closed magnetic fields trap the solar wind. These closed-field regions are surrounded by open field lines (coronal holes) along which the solar wind streams to supersonic velocities. Coronal streamers may persist for weeks to months, but at times they are the sites of spectacular eruptions known as coronal mass ejections (CMEs; Sime 1989; Burkepile & St. Cyr 1993; Hundhausen 1993). CMEs expel plasma and magnetic fields into the solar wind; the most energetic CMEs create interplanetary shock waves which in turn play a role in initiating geomagnetic storms at Earth. CMEs are thus an important link between solar and geomagnetic activity (Gosling 1993).

Understanding the initiation and evolution of CMEs has been a long-term goal of our program. The investigation of CMEs requires a model of the large-scale solar corona. Our efforts to understand CMEs have focused on first distilling the essential physics from the simplest model possible (disruption of magnetic arcades), and then incorporating these effects into more realistic models of the solar corona (including the effects of the solar wind, differential rotation, and three-dimensional geometry).

2.1.1. A Model of the Large-Scale Corona

A self-consistent description of the solar corona requires the coupled interaction of magnetic, plasma, and solar gravity forces, including the effect of the solar wind (Parker 1963). In the magnetohydrodynamic (MHD) model, the coronal plasma is described by the following equations:

$$\nabla \times \mathbf{B} = \frac{4\pi}{c}\mathbf{J}\,, \tag{1}$$

$$\nabla \times \mathbf{E} = -\frac{1}{c}\frac{\partial \mathbf{B}}{\partial t}\,, \tag{2}$$

$$\mathbf{E} + \frac{1}{c}\mathbf{v} \times \mathbf{B} = \eta\,\mathbf{J}\,, \tag{3}$$

$$\frac{\partial \rho}{\partial t} + \nabla\cdot(\rho \mathbf{v}) = 0\,, \tag{4}$$

$$\rho\left(\frac{\partial \mathbf{v}}{\partial t} + \mathbf{v}\cdot\nabla\mathbf{v}\right) = \frac{1}{c}\mathbf{J}\times\mathbf{B} - \nabla p - \nabla p_w + \rho\mathbf{g} + \nabla\cdot(\nu\rho\nabla\mathbf{v})\,, \tag{5}$$

$$\frac{\partial p}{\partial t} + \nabla\cdot(p\mathbf{v}) = (\gamma - 1)\left(-p\nabla\cdot\mathbf{v} + S\right)\,, \tag{6}$$

where **B** is the magnetic field intensity, **J** is the electric current density, **E** is the electric field, **v**, p and ρ are the plasma velocity, pressure, and mass density, **g** is the gravitational acceleration, η is the plasma resistivity and ν is the kinematic plasma viscosity. The wave pressure p_w represents the acceleration due to Alfvén waves, and is discussed in Section 2.1.9. This model is applicable to both ideal MHD, in which we set $\eta = 0$, and to resistive MHD, when η is finite.

The source term S in Eq. (6) includes coronal heating, thermal conduction parallel to **B**, radiative losses, and viscous, resistive, and Alfvén wave dissipation. A simplified model of the solar wind, known as the "polytropic model," is obtained when an adiabatic energy equation with a reduced γ is used (Parker 1963). This is a crude way of modeling the complicated thermodynamics in the corona with a simple energy equation. This choice results from setting $S = 0$ in Eq. (6) and $p_w = 0$ in Eq. (5). The primary motivation in using a reduced γ is the fact that the temperature in the corona does not vary substantially, and the limit $\gamma \rightarrow 1$ corresponds to an isothermal plasma. A typical choice is $\gamma = 1.05$. The results described in Sections 2.1.1–2.1.8 were obtained with this simplified model. While this model matches many features of the corona, it is not accurate enough to quantitatively reproduce the properties of the solar wind. In Sections 2.1.9 and 2.1.10 we describe more sophisticated models based on an improved treatment of the physical mechanisms that describe the transport and interchange of energy in the corona and solar wind (including coronal heating, thermal conduction, radiation loss, Alfvén waves and multiple ion species).

We have developed a three-dimensional code to solve the MHD Eqs. (1)–(6) in spherical coordinates. This code is described by Mikić and Linker (1994), and can be used to model the two-dimensional (axisymmetric) and three-dimensional corona, including the solar wind, differential solar rotation, the interplanetary medium (from the Sun to 1 AU), and the effect of emerging flux. Our model includes the important effect of photospheric motions on coronal magnetic fields. Because coronal magnetic fields are anchored ("line-tied") in the dense photosphere (Einaudi & Van Hoven 1983), these motions can shear and distort the field, leading to the build-up of electric currents in the corona and the energization of the magnetic field.

In order to compare our results with observations, we have calculated observable quantities from our simulations whenever possible. Coronagraphs typically measure white light scattered from coronal electrons, a quantity known as polarization brightness (pB) that is proportional to the plasma density. We calculate the polarization brightness from our simulations by integrating the plasma density along the line of sight with the appropriate scattering function (Billings 1966). In the following sections we describe the application of this code to several problems of interest in large-scale coronal physics.

2.1.2. Disruption of Magnetic Arcades

CMEs are believed to be initiated by sudden releases of energy stored in the coronal magnetic field. Both theoretical and observational studies (Priest 1988; Harrison *et al.* 1990) suggest that CMEs may be initiated from the destabilization of large-scale coronal configurations, but the mechanism by which energy in the coronal field is released is not well understood. Two explanations have been proposed. On one hand, recent theoretical calculations suggest that CMEs can be initiated by the effect of magnetic nonequilibrium produced by the distortion of magnetic field lines by photospheric shear (Mikić & Linker 1994; Roumeliotis, Sturrock & Antiochos 1994; Linker & Mikić 1995). The photospheric shear can result from differential rotation (Linker, Mikić & Schnack 1994; see Section 2.1.5). On the other hand, a recent study of the correspondence between disappearing filaments (used as proxies for CMEs) and neighboring emerging flux (Feynman & Martin 1995) implies that CMEs may be initiated by emerging flux. The relative roles of these two effects in the initiation of CMEs awaits observational confirmation.

In order to study the *theoretical* aspects of CME initiation, we used the simplest model possible: we assumed zero beta [i.e., magnetic forces dominate plasma forces, so that we can

neglect ∇p in Eq. (5)], a fixed density, neglected gravity, and only modeled the two-dimensional variation. We investigated the dynamical evolution of an initially dipolar magnetic field arcade subjected to photospheric shearing motions. The calculations were performed in axisymmetric spherical geometry, using both the ideal and resistive MHD equations. When an arcade is subjected to a photospheric shear-flow profile, the arcade evolves quasi-statically for small amounts of shear. However, beyond a critical shear, the field expands rapidly and produces a concentration of the electric current density. An ideal MHD (i.e., zero resistivity) calculation shows that a transition to a partially open configuration occurs at the critical shear value. In this state a small fraction of the magnetic field lines are closed but the majority of field lines are open. The open field lines of opposite polarity are separated by a tangential discontinuity. The magnetic energy of this partially open configuration is close to but less than the energy in a fully open field (Aly 1984, 1991; Sturrock 1991).

The transition to a partially open field requires an initially smooth magnetic field to evolve into one with discontinuities; this process has been described as magnetic nonequilibrium (Parker 1972, 1979; Priest 1981; Vainshtein & Parker 1986). The appearance of a discontinuity implies that even a small amount of plasma resistivity is important. When we included finite resistivity, the discontinuity was resolved into a current sheet which was subsequently the site of rapid magnetic reconnection, leading to fast flows and the ejection of a plasmoid (Mikić & Linker 1994). These results imply that CMEs may be initiated by the destabilization of magnetic arcades by photospheric shear.

2.1.3. Modeling Helmet-Streamer Equilibria

The relatively simple arcade model described in Section 2.1.2 allowed us to identify the underlying cause of the disruption of magnetic configurations. However, a comparison with CME observations requires the important effect of the solar wind to be included. Pneuman and Kopp (1971) developed the first 2-D model of helmet-streamer equilibria by solving the steady-state MHD equations. Our approach, and that used in many other calculations, is to integrate the time-dependent MHD equations to steady state (Steinolfson, Suess & Wu 1982; Linker, Van Hoven & Schnack 1990; Wang *et al.* 1993). These calculations require the specification of the density, temperature, and radial magnetic field at the coronal base as boundary conditions. Typically, a potential magnetic field and a transonic wind solution (Parker 1963), consistent with the specified boundary values, are chosen for the initial condition. The MHD equations are then integrated in time until the plasma and magnetic fields settle into equilibrium. The final state has a closed magnetic field region, where the plasma is trapped, surrounded by open fields, where the solar wind flows freely. Figure 1(a) shows the magnetic field configuration for a temperature of 1.6×10^6 ° K and an electron density of $10^8/\mathrm{cm}^3$ at the coronal base, with a dipole flux distribution. A current sheet bounds the closed-field region and separates the fields of opposite polarity above the closed field.

2.1.4. Disruption of Helmet Streamers

To investigate the stability of this configuration, we introduced photosphere shear flows and continued our time integration of the resistive MHD equations. Figure 1(b–f) shows projections of the magnetic field lines for the helmet streamer during the subsequent evolution. In response to the applied shear flow, the closed-field region initially expands slowly as the field evolves quasi-statically (Fig. 1a–b); when a critical shear is reached, the magnetic field lines erupt outward (Fig. 1c–d), driving plasma into the outer corona; eventually, magnetic reconnection occurs, disconnecting the plasmoid from the solar surface (Fig. 1e–f). The

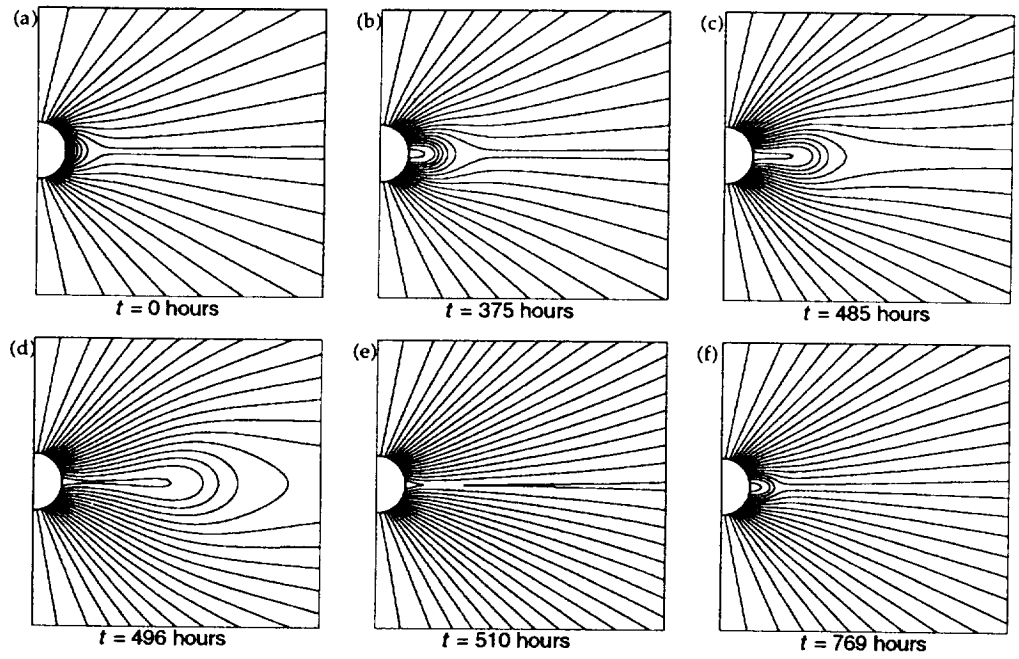

Figure 1. Evolution of an axisymmetric helmet streamer in response to photospheric shear. Past a critical shear, the helmet streamer disrupts, ejecting a plasmoid into the solar wind. This represents a simplified model of CME initiation.

evolution of the helmet streamer is in many respects similar to the dipolar arcade. However, the plasmoid formed in the streamer disruption continues to accelerate to the local solar wind speed, whereas the plasmoid in the arcade decelerates after its initial rise. While the underlying reason for the disruption is the same in both cases (ideal MHD magnetic nonequilibrium), once the streamer begins to rise, the plasma within it accelerates into the solar wind, stretching and opening the magnetic field lines, and creating a current sheet at which the low-lying loops subsequently reconnect (Linker & Mikić 1995). As the reconnection proceeds, the closed-field region grows in size as successively higher loops reconnect (Kopp & Pneuman 1976), a phenomenon that has been observed in Yohkoh soft X-ray images (Hiei, Hundhausen & Sime 1993; Tsuneta 1996).

2.1.5. The Initiation of CMEs by Differential Rotation

The studies in Sections 2.1.2 and 2.1.4 used idealized photospheric flow profiles to induce the magnetic shear. One component of photospheric motion that may contribute to the energization of large-scale coronal fields is differential rotation. We have investigated how differential rotation affects axisymmetric coronal fields over many rotations. First, we develop a helmet streamer that is not symmetric in latitude by specifying a magnetic flux distribution on the Sun and computing an equilibrium in the manner described in Section 2.1.3. We then use an observed differential rotation profile (Snodgrass 1983) to compute the evolution for several solar rotations. As in the case of the idealized shear profile, the streamer disrupts when a critical shear is exceeded. With continued differential rotation, the streamer disrupts recurrently. Figure 2 shows one of the disruption events. The results are described by Linker, Mikić and Schnack (1994) and Linker and Mikić (1995). A more complete understanding of the role of differential rotation in initiating CMEs will require three-dimensional calculations with more realistic fields.

Figure 2. Disruption of an axisymmetric helmet streamer by differential solar rotation. Projected magnetic field lines (shown in black) have been over laid on the simulated polarization brightness (large values in white, small values blue).

2.1.6. Propagation of a CME to 1 AU

One paradigm for the cause of terrestrial magnetic storms is the passage of a CME launched from the Sun past the Earth's orbit (Gosling 1993). To investigate the evolution of CMEs in the solar wind, we have used our model to form and disrupt a helmet streamer and to follow its trajectory through interplanetary space past 1 AU, including the effects of solar rotation. First an equilibrium is computed: the configuration relaxes to a steady state after approximately 3.8 solar rotations (~ 100 days). The helmet-streamer structure near the Sun is essentially the same as in the case without rotation, but far from the Sun the expected spiral structure of the interplanetary magnetic field appears (Fig. 3). The introduction of photospheric shear causes the streamer to disrupt, ejecting a plasmoid that propagates to 1 AU and perturbs the interplanetary magnetic field (IMF). Such calculations may help to predict the effect of CMEs on the IMF at Earth. The present axisymmetric calculation is only a "proof of principle" for future heliospheric calculations; we plan to repeat this calculation in 3D in the future.

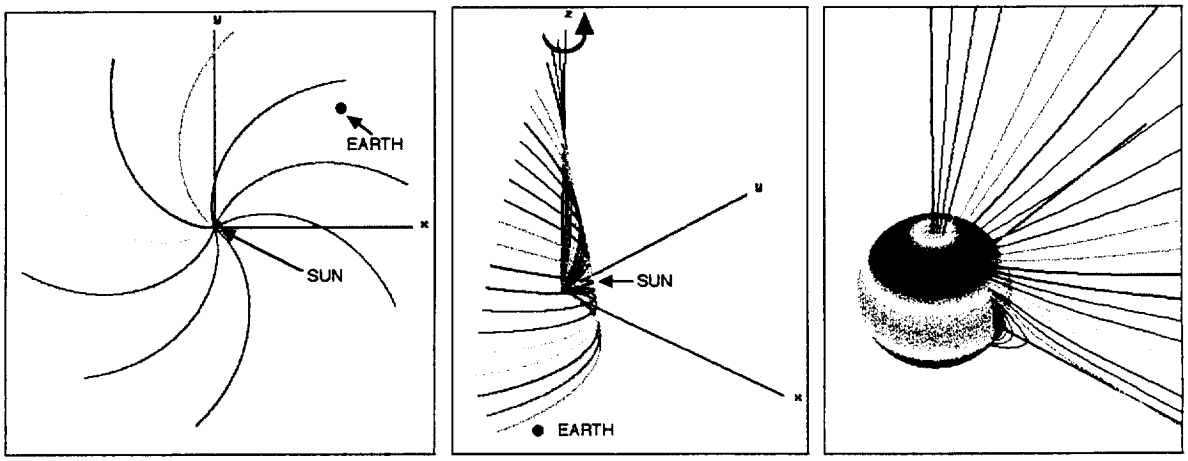

Figure 3. Spiral magnetic field produced by solar rotation. Note the closed field lines near the Sun that outline a helmet streamer.

2.1.7. Comparison with Eclipse and Coronagraph Observations

Recently we have improved our helmet-streamer calculations to allow realistic three-dimensional models of the large-scale corona to be computed (Mikić & Linker 1995). To perform these calculations, we used Wilcox Solar Observatory synoptic maps (collected during a solar rotation by daily measurements of the line-of-sight field at central meridian) to specify the radial magnetic field at the photosphere. This field is used as a boundary condition to compute a potential field in the corona. This potential field and a Parker wind solution (with uniform T and ρ at the coronal base) again specify the initial condition for the plasma, and a self-consistent 3-D solar-wind solution is developed by integrating the MHD equations in time to steady state. The solution shows the formation of helmet streamers with closed magnetic fields that trap the coronal plasma flowing out of the Sun (see Fig. 4). This solution provides a reasonably complete description of the state of the solar corona, including the detailed distribution of magnetic fields, electric currents, and coronal density and temperature.

Such solutions can reproduce the observed structures that are seen in coronagraph images and eclipse photographs of the corona. Figure 5 shows a comparison between the polarization brightness predicted by the MHD simulation and an eclipse image taken on November 3, 1994, in Chile (Mikić & Linker 1995). A comparison with Mauna Loa MK3 coronagraph observations during the solar rotation surrounding the eclipse (Carrington rotation 1888) confirms that the basic large-scale three-dimensional structure of the streamer belt has been captured in the model (see Figure 6). Such a comparison indicates that the most significant portion of the large-scale structure of the solar corona, including the position and shape of the helmet streamer belt, is determined by the magnetic field distribution on the Sun.

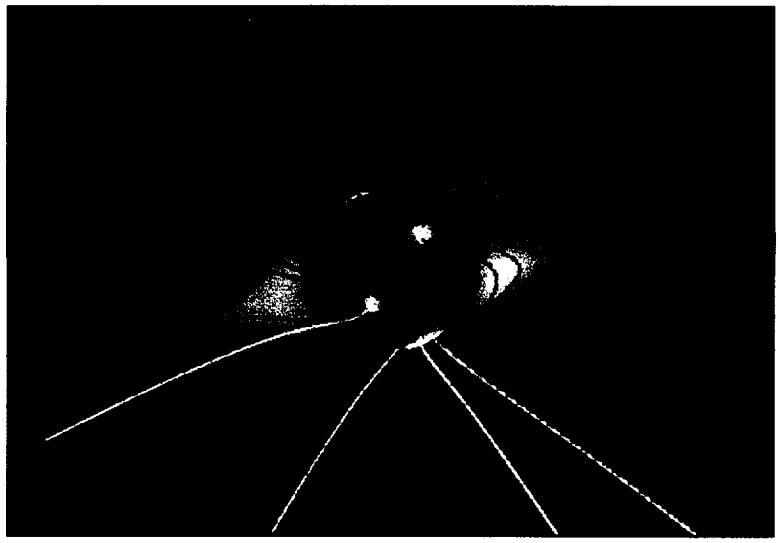

Figure 4. A three-dimensional MHD model of the structure of the solar corona during Carrington rotation 1888 (Oct–Nov 1994). The traces of the magnetic field lines show the streamer belt (closed field lines) and coronal holes (open field lines). The simulated polarization brightness (white corresponds to high coronal densities, blue to low densities) shows that helmet streamers observed on the disk correspond to closed-field regions.

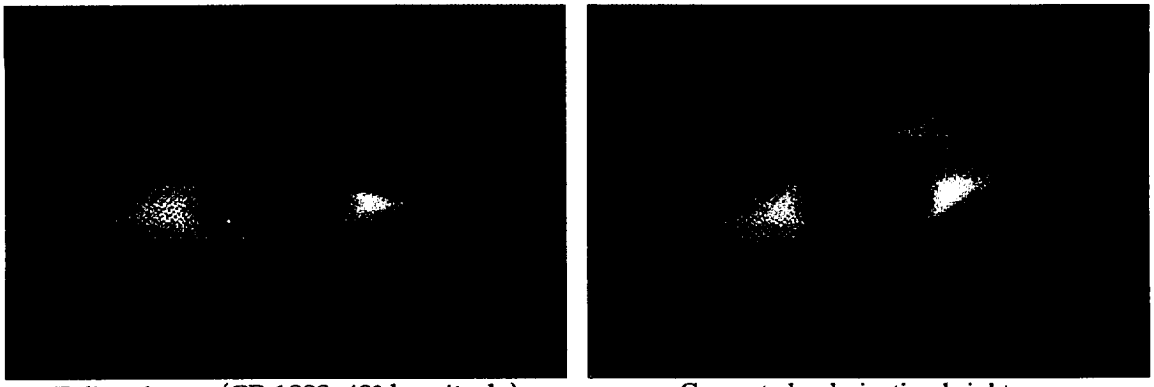

Eclipse image (CR 1888, 40° longitude)

Computed polarization brightness (MHD simulation)

Figure 5. Comparison of the coronal structure observed during the solar eclipse of November 3, 1994 with an MHD model of the corona. The white-light eclipse photo is compared with the computed polarization brightness from the MHD simulation. [Photo courtesy of the High Altitude Observatory.]

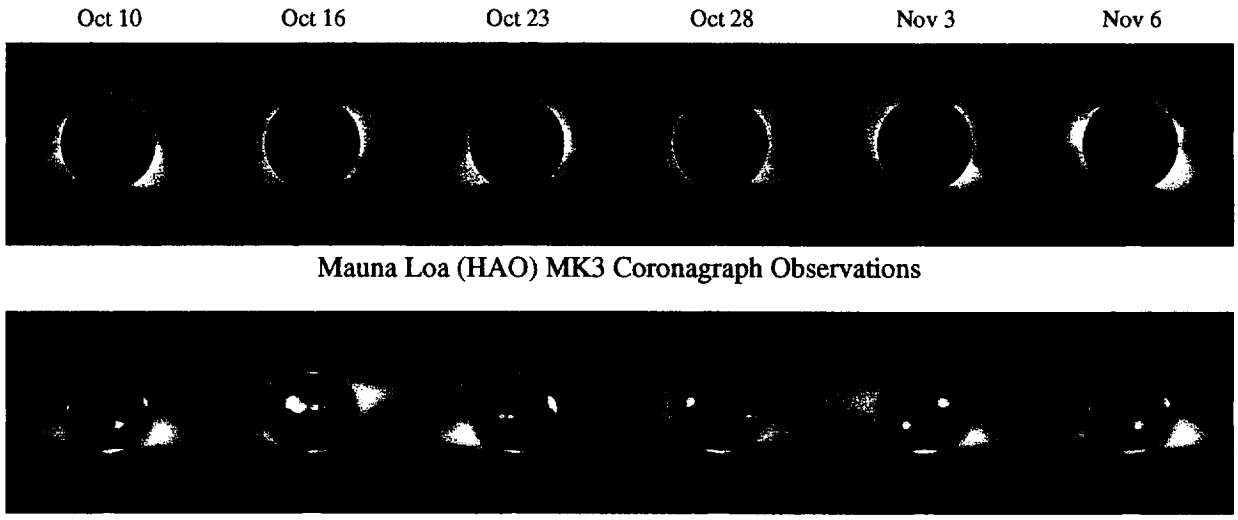

Figure 6. Comparison of the polarization brightness from an MHD simulation of the solar corona with observations taken with the Mauna Loa Solar Observatory (HAO) MK3 coronagraph, for Carrington rotation 1888 (Oct–Nov 1994).

As a further test of our coronal modeling capability, we predicted the large-scale structure of the solar corona during the October 24, 1995 eclipse (which occurred during Carrington rotation 1901). We carried out a simulation using photospheric magnetic-field data from the previous rotation (Carrington rotation 1900, Sept. 2–29, 1995) on October 5, 1995, and put the results on the World Wide Web (http://www.saic.com/home/solar/prediction.html). We also presented the results at the Sacramento Peak workshop on October 18, 1995 (described by Linker *et al.* 1996). Figure 7(a) shows tracings of the magnetic field lines for this simulation. Note that the predicted polarization brightness, shown in Fig. 7(b), agrees well with the eclipse photograph, shown in Fig. 7(c), taken by F. Diego and S. Koutchmy in Vietnam.

Figure 7. A prediction of the structure of the solar corona during the Oct. 24, 1995 solar eclipse. The MHD simulation was carried out on Oct. 5, 1995 using Wilcox synoptic magnetic data for the previous rotation. (a) Field lines and (b) polarization brightness computed from the simulation. (c) Eclipse photograph taken in Vietnam by Diego and Koutchmy in white light with f=910 mm and a two-second exposure time.

2.1.8. Comparisons With Interplanetary Observations

The coronal magnetic field not only defines the structure of the solar atmosphere, but the position of the heliospheric current sheet, and the regions of fast and slow solar wind as well. Understanding how the Sun influences the structure of the inner heliosphere requires an accurate mapping of the photospheric magnetic field into the corona and beyond.

Source-surface models (Schatten *et al.* 1969; Altschuler & Newkirk 1969; Hoeksema 1984, 1991; Wang & Sheeley 1992) make direct use of observed photospheric magnetic fields, and provide predictions of the structure of the magnetic field in the corona and heliosphere. Source-surface models have yielded important insights into the structure of the heliosphere, but several aspects of the Ulysses data are not described well by these models (Smith *et al.* 1993, 1995; Balogh *et al.* 1995). In particular, the radial magnetic field and the extent of the heliospheric current sheet predicted by source-surface models show significant discrepancies from Ulysses observations.

Just as we compared the polarization brightness predicted by our MHD computations with observations in the near-Sun corona, we have also compared the latitudinal variation of the radial magnetic field and the position of the current sheet, taken from our MHD simulation, with both source-surface model predictions and Ulysses observations. Figure 8 shows the heliospheric current sheet predicted by our MHD computation for Carrington rotation 1869 (May–June 1993), and by the source-surface model. During this time period the Ulysses spacecraft, which was located at 30°S latitude, did not cross the heliospheric current sheet (Smith *et al.* 1993). The "original" Wilcox source-surface model predicted that Ulysses *would* cross the heliospheric current sheet, whereas the MHD simulation correctly predicted no crossing. The radial magnetic field from the MHD computation shows a much smaller latitudinal variation, consistent with Ulysses observations, than it does in the source-surface model. These initial comparisons (Linker, Mikić & Winterhalter 1995) with Ulysses data indicate that our MHD computations may provide a better way of mapping dynamic structures in the solar wind back to their origins in the corona.

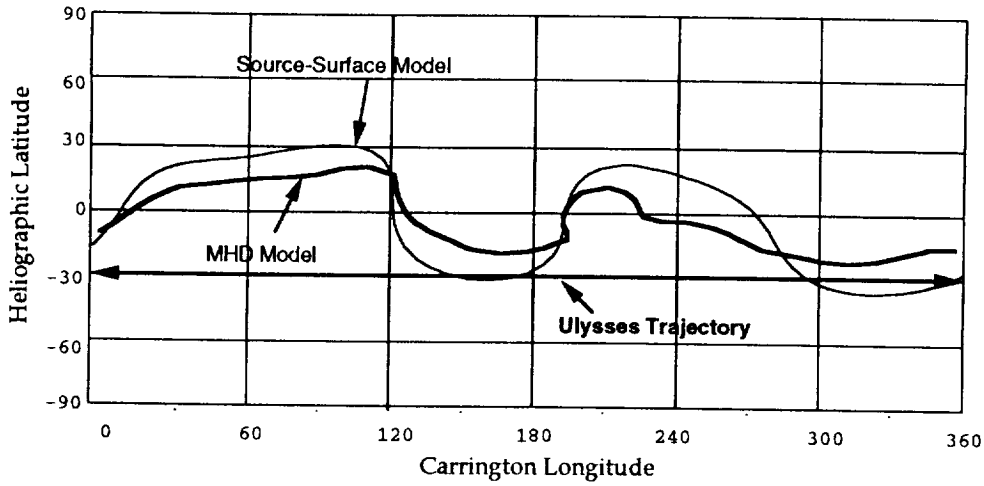

Figure 8. A comparison of the heliospheric current sheet predicted by the source-surface model and an MHD calculation for Carrington rotation 1869 (May–June 1993). The Ulysses spacecraft, which did not observe the current sheet during this rotation, was situated at 30°S latitude.

2.1.9. An Improved Solar Wind Model

In Sections 2.1.7 and 2.1.8 we demonstrated that our present MHD model compares favorably with important aspects of coronal and heliospheric data. In particular, we have confirmed the long-held belief that it is the interaction of the solar wind with coronal magnetic fields that creates the large-scale streamer structures that are observed with coronagraphs. However, when we extend our solutions to 1 A.U., we find that our model does not reproduce some of the properties of the solar wind. Improvement of the calculations requires detailed models of the physical mechanisms that control the transport and interchange of energy in the corona and solar wind.

Starting at the photosphere and rising upward into the solar atmosphere, the temperature rises steeply in the chromosphere and transition region as a result of coronal heating. It is important to note that the detailed coronal heating mechanism is not yet understood (for a recent review see Parker 1994). In the inner corona, the large parallel thermal conductivity tends to make the temperature relatively uniform (on the order of 1–2 million degrees K). The density at the top of the transition region is determined by the balance between radiation loss in the chromosphere and heating by thermal conduction from the hot corona (Withbroe 1988). As we extend into the outer solar corona and interplanetary medium, the temperature decreases slowly as a result of solar wind acceleration and thermal conduction losses. Beyond ~ $10R_S$ (where R_S is the solar radius), the plasma becomes collisionless, reducing the thermal conduction (Hollweg 1978). In this region, wind acceleration by Alfvén waves can be important, and may be necessary to produce the observed fast solar wind at 1 A.U.

In the model described in Section 2.1.1, the use of an adiabatic energy equation with a reduced polytropic index γ is an attempt to combine all of these effects into a simple model. However, not surprisingly, this formulation fails to reproduce the fast (~ 800 km/s) and slow (~ 400 km/s) wind streams that are measured at 1 A.U., as well as the temperature and density of the solar wind plasma. In particular, the polytropic model yields a latitudinal variation of the solar wind speed at 1 A.U. that is only on the order of 20%.

It is the complicated interplay of radiation loss, thermal conduction, coronal heating, and Alfvén wave acceleration and dissipation that describes the acceleration of the solar wind from the inner solar corona into the heliosphere. One-dimensional MHD models have been quite successful, despite their obvious geometrical limitations, in describing this interaction and in making comparisons with spacecraft solar wind measurements (Withbroe 1988; Habbal *et al.* 1995). It is important to recognize that some of the physical processes, such as coronal heating, must be included empirically.

The primary physical processes that must be described are the magnitude and distribution of the coronal-heating energy source, and the momentum addition to the solar wind from Alfvén waves launched at the base of the corona. In 1-D models, these processes have typically been parameterized by a coronal heat flux and dissipation scale length, and an Alfvén-wave energy flux. Extending this idea to three dimensions requires specification of the variation of these parameters between closed and open field regions.

The prescription for an improved solar wind model follows naturally from existing 1-D models. The inclusion of the effects of radiation loss, thermal conduction, coronal heating, and Alfvén-wave transport in the energy and momentum equations into a 3-D MHD model, coupled with magnetic field measurements, would eliminate the erude parameters in the 1-D models that specify the flux-tube geometry (the so-called "expansion factor"). In this formulation, the magnetic field geometry (i.e., the location and distribution of open and closed field regions) would be determined self-consistently. In addition, the balance of radiation loss and thermal conduction within the chromosphere and transition region determines the density at the base of the corona from the condition (Withbroe 1988)

$$C n_e^2 T_o^2 \int_{T_{ch}}^{T_o} Q(T) T^{1/2} dT = \tfrac{1}{2} q_o^2(T_o) \,, \tag{7}$$

where n_e is the density at the base of the corona, C is a known constant, $q_o(T_o)$ is the thermal-conduction heat flux at T_o, and the integral is performed from the base of the chromosphere (at $T_{ch} \approx 6000°K$) through the top of the transition region (at $T = T_o$). The inner boundary is now chosen to be within the transition region, at a temperature of $T_o = 500{,}000°K$. Equation (7) then yields the plasma density. The boundary conditions on the velocity are determined from the characteristic equations (Linker & Mikić 1995; Mikić & Linker 1995; Linker *et al.* 1996). Finally, in this formulation, the only boundary conditions required from observations at the base of the corona $r = R_s$ are those on the radial magnetic field.

The energy Eq. (6) thus becomes

$$\frac{\partial p}{\partial t} + \nabla\cdot(p\mathbf{v}) = (\gamma - 1)\left(- p\nabla\cdot\mathbf{v} - \nabla\cdot\mathbf{q} - n_e n_p Q(T) + H_{ch} + H_d + D \right) , \tag{8}$$

where $\mathbf{q} = -\kappa_{||}\hat{\mathbf{b}}\hat{\mathbf{b}}\cdot\nabla T$ is the parallel heat flux, $\hat{\mathbf{b}}$ is the unit vector along $\mathbf{B}$, H_{ch} is the coronal heating source, D is the Alfvén-wave dissipation term, n_e and n_p are the electron and proton densities, and $Q(T)$ is the radiation-loss function (Rosner *et al.* 1978). The term $H_d = \eta J^2 + \nu\nabla\mathbf{v}:\nabla\mathbf{v}$ represents heating due to viscous and resistive dissipation. (In the present application, H_d can be neglected, since the coronal heating term is already being parameterized.) The parallel thermal conductivity $\kappa_{||}$ is the Spitzer value in the collisional regime, $\kappa_{||} = 9 \times 10^7\, T^{5/2}$ [erg/cm^2/s], with T in degrees K, and is reduced appropriately (Hollweg 1978) in the collisionless regime beyond ~ $10R_s$. The coronal heating source is a parameterized function, as described above. For example, a particular form is

$$H_{ch} = H_0(\theta) \exp\left[-(r - Rs)/\lambda(\theta)\right] , \tag{9}$$

where $H_0(\theta)$ expresses the latitudinal variation of the volumetric heating, and $\lambda(\theta)$ expresses the latitudinal variation of the dissipation scale length. [In practice, the variation would more appropriately be expressed in terms of the magnetic topology (i.e., a proxy for the open and closed field regions) rather than simply by the latitude θ.]

The acceleration of the solar wind by Alfvén waves occurs on spatial and time scales that are below the resolution of our global numerical model. Therefore, this sub-grid-scale effect is included by using an equation for the space-time averaged Alfvén-wave energy density ε (Jacques 1977),

$$\frac{\partial \varepsilon}{\partial t} + \nabla \cdot \mathbf{F} = \mathbf{v} \cdot \nabla\, p_w - D , \tag{10}$$

where $\mathbf{F} = (\frac{3}{2}\,\mathbf{v} + \mathbf{v}_A)\varepsilon$ is the Alfvén-wave energy flux, $\mathbf{v}_A = \pm\hat{\mathbf{b}} v_A$, $v_A = B/\sqrt{4\pi\rho}$ is the Alfvén speed, and $p_w = \frac{1}{2}\varepsilon$ is the Alfvén-wave pressure. In a multi-dimensional implementation, it is necessary to transport two Alfvén wave fields: the field ε^+, which represents waves with $\mathbf{v}_A = +\hat{\mathbf{b}}\, v_A$, parallel to $\mathbf{B}$, and the field ε^-, with $\mathbf{v}_A$ anti-parallel to $\mathbf{B}$, which are combined to give ε. The wave energy density ε is related to the space-time average of the fluctuating component of the magnetic field δB by $\varepsilon = <\delta B^2>/4\pi$. The term $\mathbf{v}\cdot\nabla\, p_w$ in Eq. (10) is the work done on the Alfvén waves by the plasma flow. The wave pressure p_w also appears in the momentum Eq. (5), and expresses the force exerted on the plasma by Alfvén waves. Finally, the dissipation term D expresses the nonlinear dissipation of Alfvén waves in interplanetary space and is modeled phenomenologically (Hollweg 1978).

We have already incorporated this model in a 1-D code, and have reproduced the results of Withbroe (1988). An analysis of this 1-D model shows that it is necessary to include Alfvén waves in order to reproduce spacecraft measurements of fast solar-wind streams. It appears that without Alfvén waves it is not possible to simultaneously match measurements of solar wind temperature, density and flow velocity (Withbroe 1988).

We have also implemented these equations in a 2-D (axisymmetric) model. This self-consistent description of the energy transport in the corona has only a limited number of parameters, and represents a significant advance in coronal modeling. In our 2-D model (Mikić, Linker & Colborn 1996), we have confirmed that the complicated interaction between radiation loss in the chromosphere and lower corona, coupled with energy transport through parallel (to **B**) thermal conduction in the presence of diverging flux tubes in coronal holes, gives the observed density contrasts (up to factors of 5–10) between coronal holes and streamers as was first shown with 1-D models (Withbroe 1988). In the polytropic model, the density in the coronal holes was too high, resulting in a density contrast between holes and streamers that is only a factor of approximately 2. The improved model naturally reproduces the observed contrast, largely as a result of the radiation-balance condition, Eq. (7).

2.1.10. A Dynamic Three-Fluid Solar Wind Model

Recent Ulysses measurements have shown that there are significant differences in the dynamics and thermodynamics of the ionic components of the solar wind. Equally significant are differences in the flows as a function of solar latitude. The latter phenomena imply differences in flow parameters caused by magnetic field topology and flux-tube geometry. Since these observations may yield significant clues to the primary energy, momentum and mass inputs

to the solar wind, we have proceeded with the development and application of a fully time-dependent, three-fluid, solar-wind simulation model.

The first focus of our analyses was a comparison with the static three-fluid models of Bürgi (1992). While we have been able to re-create many of the gross features of these models, we have found some disparities due to both the nature of our code (we allow time-dependence and can only find dynamically *stable* winds) and the adoption of slightly different boundary conditions at the solar surface. Our conclusions are as follows:

1. Heating the wind, as Bürgi did, by adding energy only to the electron gas is relatively inefficient, with only about 2% of the added energy going into kinetic energy of the outflow. Most of the heat input is thermally conducted back to the solar surface (where it is radiated by the chromosphere).
2. We concur with Bürgi that the overall sensitivity of the models to changes in input parameters is due to the nonlinear behavior of the Coulomb collision terms.
3. Flux-tube topology is important. We have examined 'open' (faster-than-radial expansion for modeling coronal holes) and 'quasi-closed' (slower-than-radial expansion for simulating helmet streamers) topologies. The lower particle densities in open tubes lead to flows in which the heavy ions (alpha particles) are uncoupled from the protons and flow outward at significantly slower velocities, whereas the higher particle densities in 'quasi-closed' tubes lead to strongly coupled flows in which the alphas and protons have the same outflow speeds.
4. Careful attention must be paid to the inner boundary condition in order to include realistic model chromospheres.
5. We find larger terminal velocities (~ 400 km/sec) in our models as compared to Bürgi. Preliminary results of these simulations have been presented at the recent Solar Wind 8 conference (Ruden *et al.* 1995).

Our continuing work is now aimed at two goals: better definition of a quasi-chromospheric region where mass, energy and momentum can be added to the three species; and a comparison of ionic energization models using specific acceleration and heating theories (e.g., Axford & McKenzie 1995, and the preceding subsection).

2.2. Three-Dimensional Models of Active Region Fields

We now describe our 3-D models of magnetic fields in active regions, and compare our results with *Hα* flare observations and Yohkoh soft-X-ray telescope (SXT) measurements of the solar corona.

2.2.1. Deducing Coronal Magnetic Fields from Vector Magnetograms

The force-free approximation $\mathbf{J} \times \mathbf{B} = 0$ provides a good description of the quasi-static evolution of the strong magnetic field above an active region. Therefore, the current is assumed everywhere parallel to the field, $\mathbf{J} = \alpha\mathbf{B}$, which implies that the magnetic field satisfies the nonlinear equation

$$\frac{c}{4\pi} \nabla \times \mathbf{B} = \alpha \mathbf{B} \ . \tag{11}$$

This equation needs to be solved with the appropriate boundary conditions at the photosphere. The torsion $\alpha = \alpha(\mathbf{x})$, which obeys the equation $\mathbf{B}\cdot\nabla\alpha = 0$, is to be determined as part of the solution. An "evolutionary technique" has been developed to solve this nonlinear boundary-value problem using an iterative scheme (Mikić & McClymont 1994). Instead of directly solving the equilibrium Eq. (11), we solve a related time-dependent problem whose steady-state solution satisfies the force-free equation and matches the boundary data. The method finds solutions by dynamically adjusting the current at the coronal boundary to match the surface measurements. This technique has been used to determine coronal magnetic fields in several active regions. Selected comparisons with observations are illustrated in the following.

2.2.2. Comparison of Computed Force-Free Fields with SXT Loops

A 5.7"-pixel-resolution magnetogram was used to deduce the coronal magnetic field of active region 7222 on July 13, 1992, by applying the evolutionary technique (Mikić & McClymont 1994). Two Stokes Polarimeter magnetograms [from Mees Solar Observatory (MSO), U. Hawaii] were merged to cover the extensive active region, which contained a complicated sunspot group. The properties and topology of the computed coronal field were compared with Yohkoh SXT observations of the active region. Figure 9 shows the comparison: there appears to be good agreement between the magnetic loops in the computed field and those seen in the SXT image.

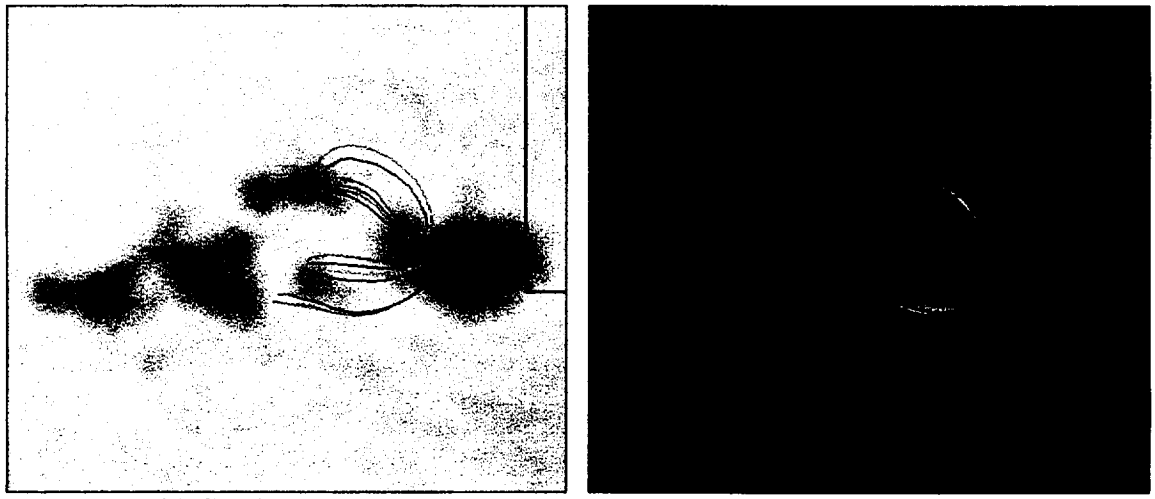

(a) Continuum Image

(b) SXT Image with Field Lines Superimposed

Figure 9. A comparison of coronal loops from the computed coronal force-free field for AR7222 and Yohkoh soft X-ray (SXT) measurements. The projected magnetic field-line traces are superimposed on (a) the continuum image, and (b) the Yohkoh SXT image. Note that the field lines appear to lie along SXT loops.

2.2.3. Morphology of Force-Free Fields Deduced from Flare Emission

We have made use of the coronal field computed from the magnetogram of active region 5747 on October 20, 1989 to compare the connectivity of the coronal field with Hα data obtained at MSO, during an M2 flare (Leka *et al.* 1993) which occurred 3 hours after the magnetogram scan was completed. In Fig. 10 the observed Hα-flare features are superimposed on the magnetogram of active region 5747; note that the footpoints of a coronal loop in the estimated

force-free coronal field are in much closer agreement with the observed high-pressure regions than footpoints of a loop in the potential magnetic field (Mikić & McClymont 1994).

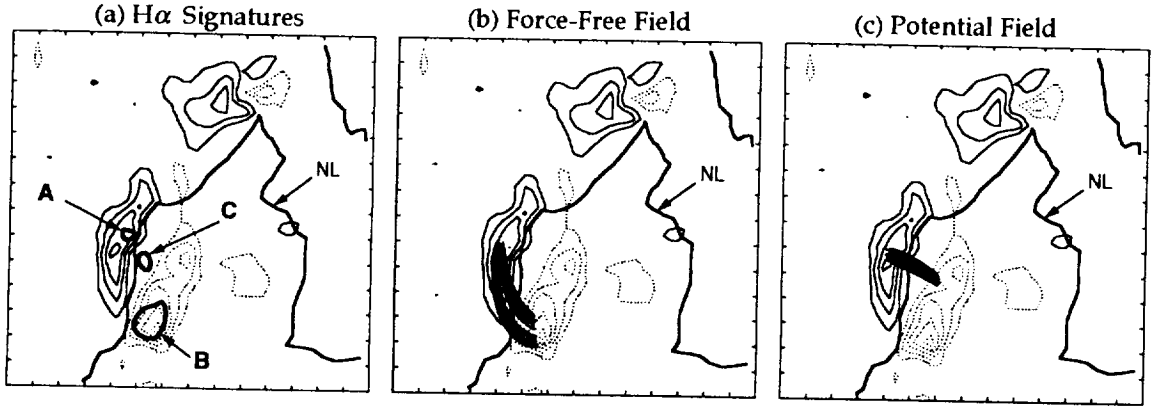

Figure 10. (*a*) Hα flare features superimposed on the magnetogram of AR5747 (adapted from Leka *et al*. 1993). The dark line marked NL denotes the magnetic neutral line; the contours denote the vertical current. The three small pseudo-circular features enclose areas in which specific Hα signatures were detected. The features marked A and B show sites which were identified as high pressure "footpoints," whereas C was identified as an electron-precipitation site and coincided temporally with hard-X-ray emission. (*b*) Field-line traces in the estimated *force-free* coronal field, showing that the high-pressure sites A and B are close to the footpoints of a coronal loop. (*c*) Field-line traces in the *potential* coronal field, with the same initial footpoint positions (at A) as in (*b*), showing that the agreement between the high-pressure sites and coronal-loop footpoints is much better for the estimated force-free field than for a crude current-free field.

2.3. The Development of Emerging Flux and Current

2.3.1. Emerging Flux and Coronal Evolution

The emergence of new magnetic flux from below the photosphere plays an important role in solar activity. Observations suggest a correlation between emerging flux and energy release in active regions (e.g., X-ray bright points), including the onset of solar flares (Leka *et al.* 1994). Emerging flux also correlates with changes in large-scale coronal structures, including filaments and coronal mass ejections (Feynman & Martin 1995). When a magnetic loop emerges from the high-beta plasma below the photosphere into the low-beta plasma in the corona (by the effect of magnetic buoyancy), it expands substantially, and interacts with the ambient magnetic fields in the corona. The orientation of the magnetic field lines in the emerging field compared to those of the ambient field determine whether magnetic reconnection will occur. Reconnection produces energy dissipation, heating, and jet flows (Shibata 1995).

In the following two sections we describe simulations of the interaction of emerging flux with coronal magnetic fields. In our computations we are primarily interested in the coronal consequences of emerging flux. Therefore, we do not model the complicated plasma interactions associated with buoyant flux tubes submerged under the photosphere (and the attendant difficulties associated with the short vertical scale lengths for sub-photospheric and chromospheric fields); rather, we specify generic flux $B_z(x,y,t)$ and current $J_z(x,y,t)$ profiles at the photosphere ($z = 0$) as a function of time, and we then calculate the self-consistent evolution of the field as it interacts with the ambient field in the corona ($z > 0$). In our code, magnetic flux is emerged by specifying boundary conditions on the tangential electric field at the photosphere. By appropriately specifying the solenoidal and transverse components of the

tangential electric field, we can emerge untwisted fields (with $J_z = 0$; see Section 2.3.2) or twisted fields (with $J_z \neq 0$; see Section 2.3.3).

2.3.2. Flux Emergence in Two Dimensions

In order to test our model of flux emergence in two dimensions, we emerged a bipole next to a pre-existing bipole of opposite sign (Linker & Mikić 1994). Figure 11 shows the evolution; magnetic reconnection occurs as the smaller bipole emerges into the corona, producing jet flows [similar to those seen by Forbes and Priest (1984) and Shibata (1995)]. In this case neither the initial bipole nor the emerging magnetic field had any shear associated with it. In the final configuration the magnetic field is nearly potential.

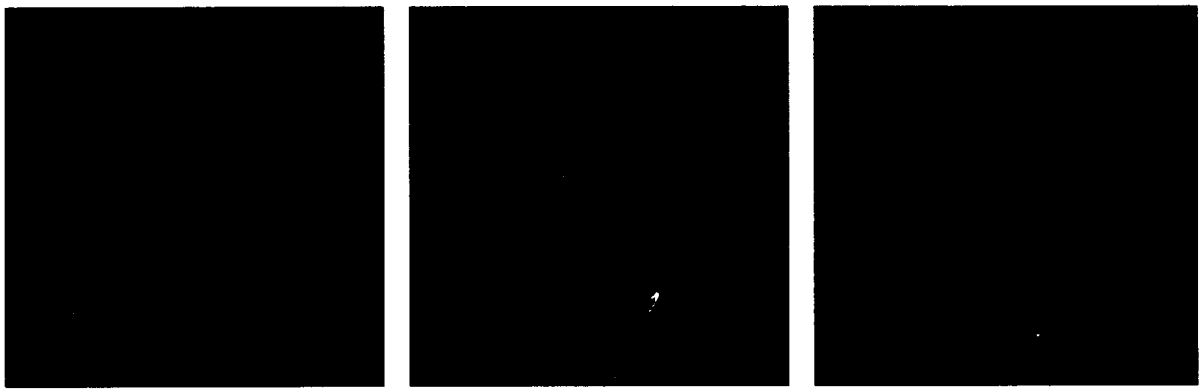

Figure 11. Interaction of an emerging bipole with a pre-existing bipole in 2D. Magnetic field lines are shown in black; the current density out of the plane is shown in color (red is positive, green is zero, blue is negative). Magnetic reconnection occurs as the smaller bipole emerges into the corona.

2.3.3. Emergence and Interaction of Magnetic Loops in Active Regions

In order to simulate flux emergence in active regions, we have developed a three-dimensional model. As a first step, we have emerged a 3-D coronal loop through the base into a field-free plasma. Current is injected into the loop by applying an electrostatic potential in the base plane. This process emerges both toroidal and poloidal magnetic-field components into the corona through a fixed (conducting) surface with loop footpoints anchored at fixed locations. Next, we take into account the effect of plasma motions on the photosphere as the magnetic field emerges by allowing the plasma to flow at the footpoints in response to magnetic forces. This degree of freedom allows the loop fields to evolve into a non-planar geometry, similar to the results obtained in our previous study (Van Hoven *et al.* 1995a) using an entirely different loop-formation mechanism. Figure 12 shows an early and late snapshot of this twisted-loop (B_z and J_z increasing) emergence (Mok *et al.* 1996).

Next, in a situation that is topologically similar to that described in Section 2.3.2 (but now in three dimensions), we have emerged an untwisted loop underneath, and at right angles to, an existing potential (untwisted) loop. The field lines in the emerging loop reconnect with the magnetic field lines in the existing loop, releasing energy. Finally, we have emerged a twisted loop under an existing twisted coronal loop, formed by vortically convecting the footpoints of a potential coronal loop (as described in Section 2.4.1). The emerging and rising twisted flux loop was generated underneath the coronal loop by specifying the appropriate tangential electric field,

as described in Section 2.3.1. The two loops eventually interact and reconnect (see Fig. 13) to reach a lower energy state, producing fast flows. Although these results are preliminary, they are typical of observations of jet flows near emerging-flux regions.

Figure 12. The emergence of a coronal flux loop. (a) At time = 100 τ_A, a bipolar magnetic field begins to emerge from the photosphere. (b) At time = 800 τ_A, as the electric current intensifies, the loop field expands upward and the field lines become helical. The motion of the footpoints distorts the loop into a non-planar geometry.

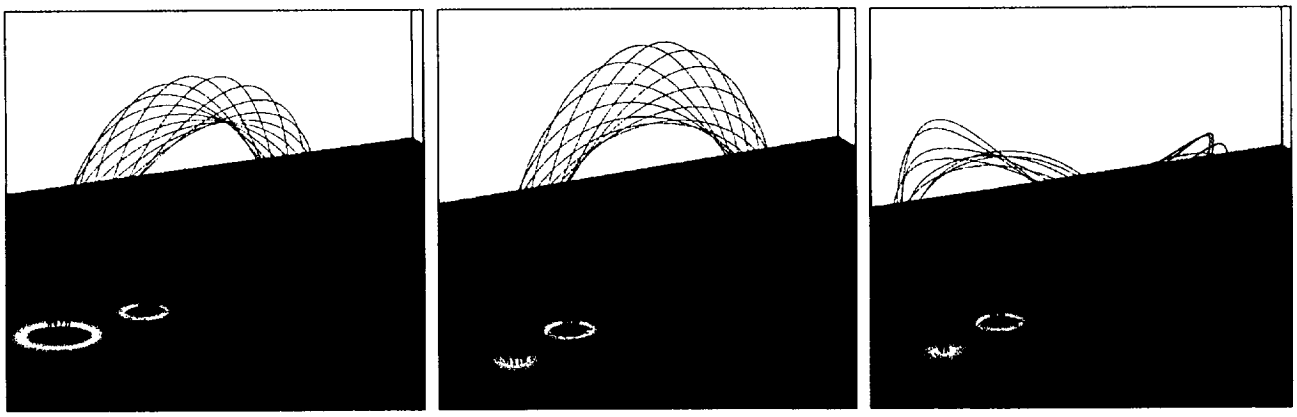

Figure 13. Interaction of a twisted emerging loop with a pre-existing twisted coronal loop. Note that the magnetic field lines in the "red" loop reconnect with those of the "black" loop, producing fast flows. The photospheric image shows the vertical magnetic field in the photosphere (red indicates positive fields, blue indicates negative fields).

2.4. Formation and Evolution of Coronal Loops

Solar coronal loops have excited interest since the Skylab era and have reappeared as a prominent feature of Yohkoh observations (Klimchuk *et al.* 1992). Their magnetic and plasma properties have also provided a continuing focus for theory and simulations (Van Hoven 1981; Mikić, Schnack & Van Hoven 1990; McClymont & Mikić 1994).

2.4.1. Formation of Stable Coronal Loops

During this grant period we have demonstrated the dynamic formation of coronal magnetic loops in three dimensions as a result of the effects of horizontal, vortex-like, photospheric convection on a pre-existing current-free bipole (Van Hoven, Mok & Mikić 1995a), as shown in Fig. 14(a). The applied photospheric twist propagates into the corona, causing parallel current to flow along an S-shaped loop. This appearance has been known from force-free-field models,

including those based on observations (McClymont & Mikić 1994; Rust 1995). The loop in Fig. 14(a), with a twist of 2.8π on the central field line, is in a stable, force-free, equilibrium state. The twisted field lines in the loop are surrounded by overlying field lines that remain relatively undistorted.

2.4.2. Dynamic Evolution of Coronal Loops

It is known that coronal loops can become unstable to kink instabilities if they are twisted sufficiently (Mikić *et al.* 1990). Furthermore, they may exhibit magnetic nonequilibrium (similar to that of coronal arcades, as described in Section 2.1.2) that would make them erupt. We have investigated the dynamic evolution of three-dimensional coronal loops under two conditions: with and without the presence of an overlying background magnetic field. In the first case, when a loop with an overlying current-free arcade field is twisted beyond the amount described in the previous subsection, the upwardly expanding loop field collides with the background field, forming a current layer in between. Continued twisting of the footpoints results in the narrowing and subsequent magnetic tearing (reconnection) of this current layer, starting at the apex, as shown in Fig. 14(b). Shibata (1995) has proposed that this type of reconnection could be a trigger for loop flares and their outflow jets, a topic that we are continuing to study.

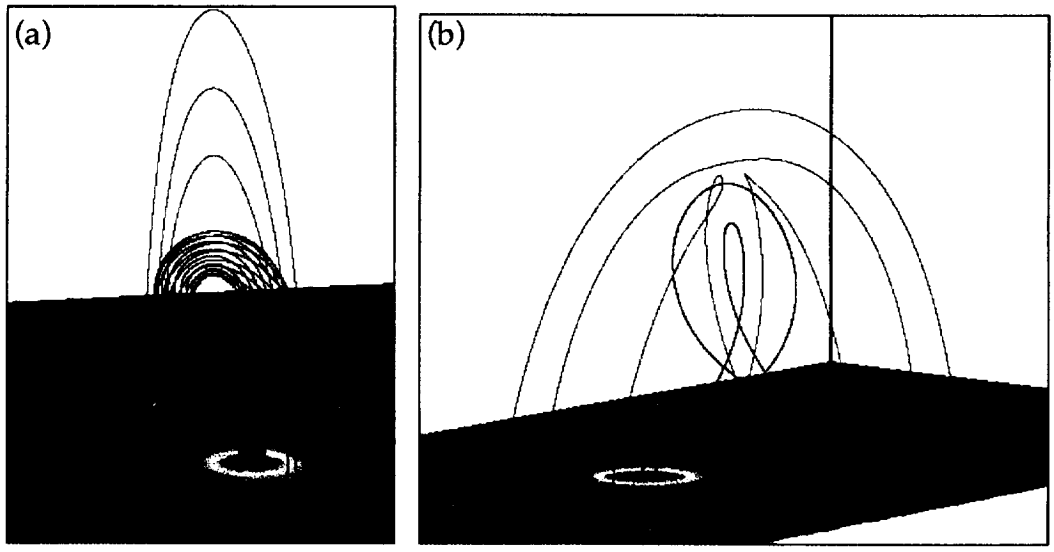

Figure 14. A coronal loop that is formed by vortical photospheric motions in the presence of an overlying arcade field. (a) A stable equilibrium loop with an axial twist of 2.8π. (b) When the loop is twisted by 4.2π, reconnection of the upper field lines occurs. Note that the magenta-colored field lines have reconnected.

The evolution of loops without an overlying magnetic field has also been examined (Van Hoven *et al.* 1995b). In this case, the magnetic loop continues to expand upward without hindrance. Together with the fact that the field lines are longer, the magnetic field strength decays rapidly with altitude, resulting in lower Alfvén speeds and longer transit times along the field lines. Our simulations have not reached an equilibrium, nor has reconnection been detected. The field lines appear to be helical and expanding in the upward direction. This case is under continuing investigation, with a planned improvement being the addition of a gravitationally stratified atmosphere.

2.5. CORONAL HEATING BY CURRENT FILAMENTS

One of the fundamental theoretical questions of solar physics is: how does the corona achieve a temperature which is much higher than that of the photosphere? By considering the measured conductive and radiative energy losses (McWhirter & Wilson 1976; Withbroe & Noyes 1977), the input energy flux required to heat the corona is estimated to be $P \sim 3 \times 10^5 erg/cm^2/s$ in the quiet corona and $P \sim 10^7 erg/cm^2/s$ in active regions. In most current models of coronal heating it is the magnetic coupling between the photospheric granular motions which provides the basic energy input that can sufficiently heat the corona.

One can calculate the Poynting-flux energy input from observed photospheric motions (Parker 1983; Hendrix *et al.* 1996) and find sufficient energy for coronal heating. The question therefore becomes, how can this energy be dissipated in the corona? Gold (1964) proposed that dissipation of electric currents generated from the photospheric Poynting flux could provide a local heating mechanism. However, electric currents, if formed on the granular length scale, cannot dissipate enough energy to account for the observed losses in active region loops. Parker (1972) then suggested that the random-walk advection of the photospheric magnetic field can drive the coronal electric current to extremely small scales, thereby providing enough dissipation to allow a power balance between resistive dissipation and the Poynting flux.

To assess the viability of Parker's (1983, 1994; van Ballegooijen 1988; Mikić *et al.* 1989; Longcope & Sudan 1994) coronal heating model we have performed a series of MHD simulation studies of the dynamical response of a magnetized resistive plasma to long-length-scale motions of the footpoints of the magnetic field lines (Schnack & Mikić 1994; Van Hoven *et al.* 1995c; Hendrix & Van Hoven 1996; Hendrix *et al.* 1996; Hendrix 1996; Schnack *et al.* 1996).

2.5.1. Fine-scale coronal structure

In our simulations, we find the Ohmic energy dissipation in Parker's model to be intermittent, with most of the heating occurring during the dynamic formation of small-scale current sheets. We found, and verified numerically, that a lower limit (for high resistivity) to the time-average Poynting flux (Hendrix *et al.* 1996; Hendrix 1996) is given approximately by

$$\overline{P} = \frac{T_0 \overline{V}_0^2 B_0^2}{L} \tag{12}$$

where T_0 is the granular coherence time, $\overline{V}_0$ is the time-averaged photospheric plasma velocity, B_0 is the axial magnetic field strength, and L is the length of the loop. Our numerical simulations have shown that, over a large range of values for the resistivity, Parker's 1972 conception was correct: the electric current will naturally form in thin sheets (Schnack & Mikić 1994; Schnack *et al.* 1996) such that there is enough resistive dissipation to balance the input Poynting flux. In fact, for lower values of the resistivity, the power input/dissipation is found to increase. Thus the question is not whether sufficiently thin current filaments will develop, but rather whether resistivity will allow the coronal field to become sufficiently stressed near the photosphere (i.e., build up sufficient $B_\perp$) to allow for enough Poynting flux to heat the corona (Parker 1983). Ironically, too much resistivity will defeat this method of heating.

Our goal has thus been to determine whether the dissipation of these current filaments can produce sufficient Ohmic power to significantly contribute to coronal heating. By inserting the range of values from Table I into (12), one can find the required $10^7 erg/cm^2/s$ necessary to explain the observed coronal energy losses. It is also encouraging that more heating occurs as S is increased toward coronal values. A strong inference from these results is that our simulations

show that (approximately) enough current density (or $B_\perp^2$) can be generated in the corona to support Parker's conclusions.

Table I: Coronal parameters. In our simulations a value of $L/L_\perp = 4$ was used.

PARAMETER NAME	PHYSICAL CONSTANT	PHYSICAL VALUE
Granular width	$L_\perp$	10^8 cm
Flux tube length	L	$10^9 - 10^{10}$ cm
Magnetic field	B_0	100 G
Plasma speed	V_0	$0.5 - 5 \cdot 10^5$ cm/s
Coherence time	T_0	$0.3 - 1 \cdot 10^3$ s
Alfvén speed	V_A	10^9 cm/s
Alfvén time	$T_A = L_\perp / V_A$	10^{-1} s

2.5.2. 3-D Rapid Magnetic Reconnection

We have developed a diagnostic (Van Hoven *et al.* 1995c) which allows, in 3D, the determination of spontaneous reconnection sites (Hesse & Schinder 1988). We find with this diagnostic that the dynamic formation of current sheets is characterized by magnetic reconnection, as shown in Fig. 15, and exponential growth of the amplitude of the parallel current (Fig. 16).The current-filament formation is fast when compared to the global time scales of the system, with an e-folding time that is approximately $3T_A$ at $S = 5000$. Furthermore, we have diagnosed the evolution of the current sheets through their growth and decay (Hendrix 1996), and find it qualitatively and quantitatively consistent with the essential features of the line-tied coalescence instability (Longcope & Strauss 1994) leading to a nonlinear reconnection/dissipation phase. The result of this instability is a rapid (ideal MHD time scale) formation of a current filament leading to magnetic reconnection which dissipates the current filaments also on a nearly ideal MHD time scale. With the possibility in mind that the current filaments might be magnetic-tearing unstable (Furth *et al.* 1963; Van Hoven & Cross 1973), we find the reconnection dissipation time scale can be understood in terms of the tearing instability and the concept of a local Lundquist number (Hendrix 1996).

2.5.3. *The Turbulent Corona*

Due to the random nature of the photospheric drive and the high value of the coronal Lundquist number S, it is likely that turbulence plays a role in the dynamics of the closed regions of the corona. We have analyzed the energy spectrum of the dynamic excitations in our simulations in an effort to understand the nature of the transfer of energy from large-scale granular motions to small-scale magnetic dissipation (Politano *et al.* 1989), and were able to find a well developed inertial range during the formation of current sheets when the Ohmic heating is relatively large (Hendrix & Van Hoven 1996). This phenomenon, shown in Fig. 16, is coincident with reconnection of the magnetic field lines during the dynamic formation and dissipation of intense localized current filaments.

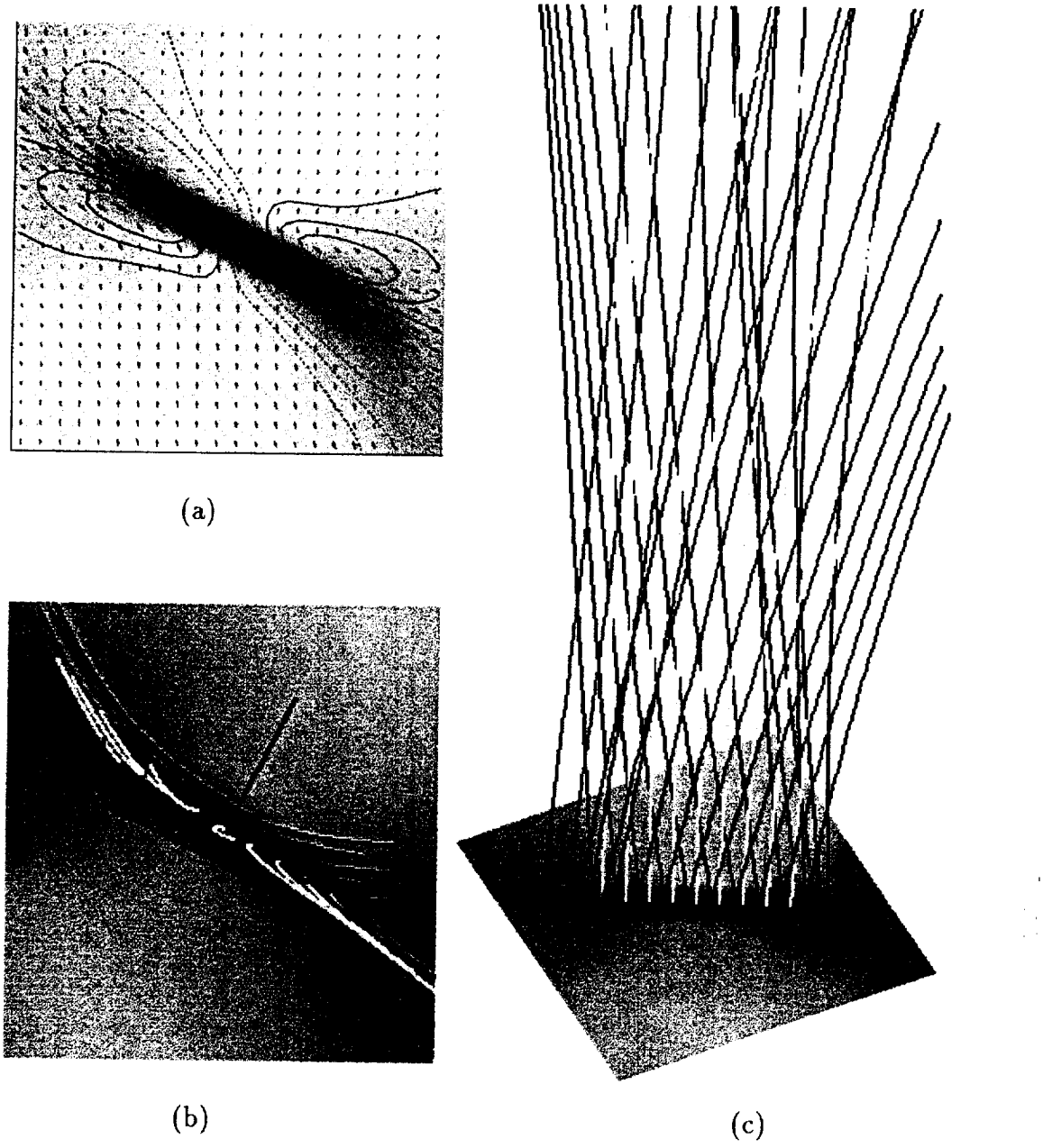

Figure 15. (a) Composite plot of parallel current density (dark shading), parallel vorticity (contours, with negative values denoted by dashed lines), and perpendicular velocity (vectors) in the loop midplane. (b) Top and (c) side views showing a selection of field lines threading the large current-density region, some of which show the characteristic X-point reconnection structure. Field lines were generated by integrating along **B** beginning in the midplane. The color of each field line signifies its origin with respect to the plane of symmetry defined by the current sheet (i.e., white lines originate in the middle of the sheet and black and gray lines originate on either side)

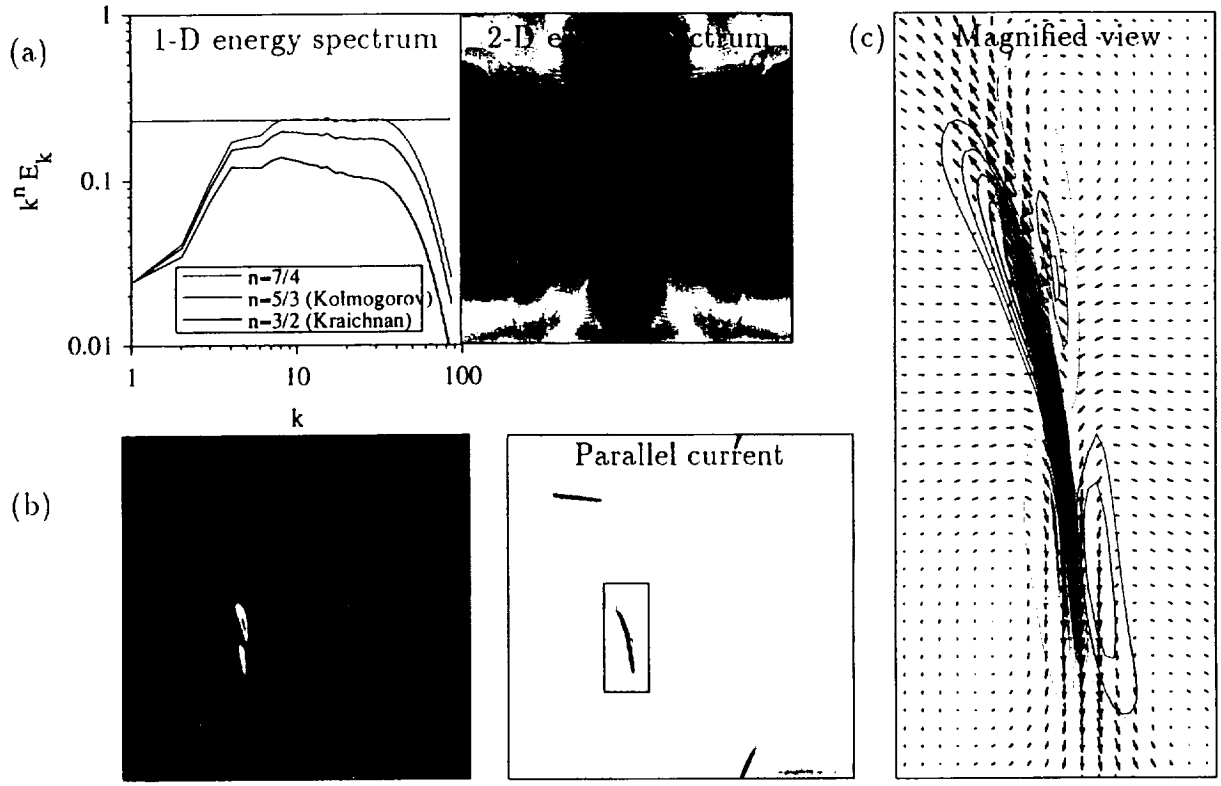

Figure 16. A reconnection event from a 3-D simulation of Parker's coronal heating model. Energy spectra (a) illustrate an inertial range and the anisotropy of the transverse-wavenumber 2-D spectrum during current-sheet formation. The transverse variation of the parallel vorticity and current density in the mid-plane of the domain are shown in (b). The magnified view (c) illustrates plasma flow vectors in the current-sheet region that are characteristic of magnetic reconnection.

As we have mentioned, these simulations were performed in a relatively resistive plasma as compared to the solar corona. At coronal values of the resistivity, the filaments will certainly be thinner than in our simulations. Therefore, as S is increased, the sheets can become unstable to secondary resistive tearing (Biskamp 1986; Biskamp & Welter 1989) so that they will break up into even smaller filaments. With the addition of low-level broad-band noise (which certainly exists in the corona), it is likely that for higher S the observed inertial range would extend to much higher wavenumbers. Thus, further fine structure will develop in the nonlinear current filaments, as was exhibited in the 2-D turbulence simulations performed by Biskamp and Welter (1989). With these concepts in mind, a coalescence/reconnection driven turbulent-relaxation process can be considered as a possible mechanism (at high S) for the ultimate dissipation of current filaments and the subsequent heating of the corona.

2.5.4. Conclusions

We have seen that the Poynting-flux energy input and the resulting Ohmic dissipation in Parker's model are approximately large enough to explain the observed energy losses in the solar corona. Of course, this assumes that Parker's model and our simulations are applicable to coronal conditions. With these caveats in mind, the simulations have shown that the required Ohmic dissipation is a result of spontaneous *dynamic* current filamentation which occurs on the Alfvén time scale as a result of the slow *quasi-static* boundary drive. Furthermore, we have

investigated the possibility that the magnetic coalescence instability is the triggering mechanism, and have found that this is indeed most probable.

On the subject of the dissipation of the current filaments, we saw that magnetic reconnection is certainly involved. As to the actual dynamic mechanism, the coalescence instability in a resistive medium leads to magnetic reconnection during the late nonlinear stages of the instability. Additionally we saw that, during filamentation events, the energy spectrum resembles that of a turbulent medium such that, at the low values of resistivity which exist in the corona, a turbulent relaxation of the current filaments will probably occur.

There is still much work to be done on this problem. One challenging topic involves the scaling laws in terms of the resistivity. In the absence of larger computers, it may be possible to run some simulations in 2D (Einaudi *et al.* 1996) to gain better resolution. However, the effect of the neglect of axial transverse Alfvén waves in this configuration must be considered carefully. It is the authors' hope that in the future we will have a much better understanding of the physics of current-filament formation in terms of the concepts discussed here.

REFERENCES

Altschuler, M. D., & Newkirk, G. 1969, *Sol. Phys.*, **9**, 131.

Aly, J. J. 1984, *Ap. J.*, **283**, 349.

Aly, J. J. 1991, *Ap. J.*, **375**, L61.

Axford, W. I., & McKenzie, J. F. 1995, "The Solar Wind", in *Cosmic Winds and the Heliosphere*, to appear; also, Solar Wind 8 Conference, Dana Point, CA, paper O-1-19.

Balogh, A., Smith, E. J., Tsurutani, B. T., Southwood, D. J., Forsyth, R. J., & Horbury, T. S. 1995, *Science*, **268**, 1007.

Billings, D. E. 1966, *A Guide to the Solar Corona*, Academic Press.

Biskamp, D. 1986, *Phys. Fluids*, **29**, 1520.

Biskamp, D., & Welter, H. 1986, *Phys. Fluids B*, **1**, 1964.

Burkepile, J. T., & St. Cyr, O. C. 1993, NCAR/TN-369+STR.

Bürgi, A. 1992, *J. Geophys. Res.*, **97**, 3137.

Carrington, R. C. 1860, *Mon. Not. R. Astron. Soc.*, **20**, 13.

Einaudi, G., & Van Hoven, G. 1983, *Sol. Phys.*, **88**, 163.

Einaudi, G., Velli, M., Pouquet, A., & Politano, H. 1995, *Ap. J. Letts.*, **457**, L113.

Feynman, J., & Martin, S. F. 1995, *J. Geophys. Res.*, **100**, 3355.

Forbes, T. G., & Priest, E. R. 1984, *Solar Phys.*, **94**, 315.

Furth, H. P., Killeen, J., & Rosenbluth, M. N. 1963, *Phys. Fluids*, **6**, 459.

Gold, T. 1964, in The Physics of Solar Flares, ed. W.N. Hess (NASA SP-50) p. 389.

Gosling, J. T. 1993, *J. Geophys. Res.*, **98**, 18937.

Habbal, S. R., Esser, R., Guhathakurta, M., & Fisher, R. R. 1995, *Geophys. Res. Lett.*, **22**, 1465.

Harrison, R. A., Hildner, E., Hundhausen, A. J., Sime, D. G., & Simnett, G. M. 1990, *J. Geophys. Res.*, **95**, 917.

Hendrix, D. L. 1996, Ph.D. Dissertation (University of California, Irvine).

Hendrix, D. L., & Van Hoven, G. 1996, *Ap. J.*, **467**, xxx.

Hendrix, D. L., Van Hoven, G., Mikić, Z., & Schnack, D. D. 1996, *Ap. J.*, **470**, xxx.

Hesse, M., & Schindler, K. 1988, *J. Geophys. Res.*, **93**, 5559.

Heyvaerts, J., & Priest, E. R. 1984, *Astron. Astrophys.*, **137**, 63.

Hiei, E., Hundhausen, A. J., & Sime, D. G. 1993, *Geophys. Res. Lett.*, **20**, 2785.

Hoeksema, J. T. 1984, Tech. Rep. CSSA-ASTRO-84-07, Center for Space Science and Astronomy, Stanford University, Calif.

Hoeksema, J. T. 1991, Tech. Rep. CSSA-ASTRO-91-01, Center for Space Science and Astronomy, Stanford University, Calif.

Hollweg, J. V. 1978, *Rev. Geophys. Space Phys.*, **16**, 689.

Hundhausen, A. J. 1993, *J. Geophys. Res.*, **98**, 13177.

Jacques, S. A. 1977, *Ap. J.*, **215**, 942.

Klimchuk, J.A., Lemen, J. R., Feldman, U., Tsuneta, S., & Uchida, Y. 1992, *Publ. Astron. Soc. Japan*, **44**, L181.

Kopp, R. A., & Pneuman, G. W. 1976, *Sol. Phys.*, **50**, 85.

Leka, K. D., Canfield, R. C., McClymont, A. N., de La Beaujardière, J.-F., Fan, Y., & Tang, F. 1993, *Ap. J.*, **411**, 370.

Leka, K.D., Canfield, R. C., McClymont, A. N., Metcalf, T. R., and Mickey, D. L. 1994, *EOS (Trans. AGU)*, **75**, 281.

Linker, J. A., & Mikić, Z. 1994, *EOS (Trans. AGU)*, **75**, 281.

Linker, J. A., & Mikić, Z. 1995a, *Ap. J.*, **438**, L45.

Linker, J. A., & Mikić, Z. 1995b, *Solar Wind 8* Conference, Dana Point, CA, paper P-1-14.

Linker, J. A., Van Hoven, G., & Schnack, D. D. 1990, *Geophys. Res. Lett.*, **17**, 2281.

Linker, J. A., Mikić, Z., & Schnack, D. D. 1994, *Proc. Third SOHO Workshop —Solar Dynamic Phenomena and Solar Wind Consequences*, Estes Park, Colorado, USA (ESA SP-373, December 1994), p. 249.

Linker, J. A., Mikić, Z., & Winterhalter, D. 1995, *EOS (Trans. AGU)*, **76**, S238.

Linker, J. A., Mikić, Z., & Schnack, D. D. 1996, in *Solar Drivers of Interplanetary and Terrestrial Disturbances* (K. S. Balasubramaniam, S. L. Keil, and R. N. Smartt, eds.), Astronomical Society of the Pacific, Conference Series, Vol. **95**, p. 208.

Longcope, D. W., & Strauss, H. R. 1994, *Ap . J.*, **426**, 742.

McClymont, A. N., & Mikić, Z. 1994, *Ap. J.*, **422**, 899.

McWhirter, R. W., & Wilson, R. 1976, *Trans. R. Soc. Lond.*, **A281**, 331.

Mikić, Z., & Linker, J. A. 1994, *Ap. J.*, **430**, 898.

Mikić, Z., & Linker, J. A. 1995, *Solar Wind 8*, Conference, Dana Point, CA, paper P-1-15.

Mikić, Z., Linker, J. A., & Colborn, J. A. 1996, *EOS Trans. AGU*, **77**, Sxxx.

Mikić, Z., & McClymont, A. N. 1994, in *Solar Active Region Evolution: Comparing Models with Observations* (K.S. Balasubramaniam and G. W. Simon, eds), Astron. Soc. Pac., Conf. Series, **68**, 225.

Mikić, Z., Schnack, D. D., & Van Hoven, G. 1989, *Ap. J.*, **338**, 1148.

Mikić, Z., Schnack, D. D., & Van Hoven, G. 1990, *Ap. J.*, **361**, 690.

Mok, Y., Van Hoven, G., & Mikić, Z. 1996, *Bull. AAS*, **28**, 875.

Parker, E. N. 1963, *Interplanetary Dynamical Processes* (New York: Wiley-Interscience).

Parker, E. N. 1972, *Ap. J.*, **174**, 499.

Parker, E. N. 1979, *Cosmical Magnetic Fields* (Oxford:Clarendon).

Parker, E. N. 1983, *Ap. J.*, **264**, 642.

Parker, E. N. 1994, *Spontaneous Current Sheets in Magnetic Fields* (New York: Oxford).

Pneuman, G. W., & Kopp, R. A. 1971, *Solar Phys.*, **18**, 258.

Politano, H., Pouquet. A., & Sulem, P.L., 1989, *Phys. Fluids B*, **1**, 2330.

Priest, E. R. 1981, in *Solar Flare Magnetohydrodynamics*, ed. E. R. Priest (London: Gordon & Breach), pp. 142 and 150.

Priest, E. R. 1988, *Ap. J.*, **328**, 848.

Rosner, R., Tucker, W. H., & Vaiana, G. S. 1978, *Ap. J.*, **220**, 643.

Roumeliotis, G., Sturrock, P. A., & Antiochos, S. K. 1994, *Ap. J.*, **432**, 847.

Ruden, S. P., Schiano, A. V. R., & Van Hoven, G. 1995, *Solar Wind 8* Conference, Dana Point, CA, paper P-1-32.

Rust, D. M. 1995, *EOS (Trans. AGU)*, **76**, S235.

Schatten, K. H., Wilcox, J. M., & Ness, N. 1969, *Sol. Phys.*, **6**, 442.

Schnack, D. D., & Mikić, Z. 1994, in *Solar Active Region Evolution: Comparing Models with Observations* (K.S. Balasubramaniam and G.W. Simon, eds), Astron. Soc. Pac., Conf. Series, **68**, 180.

Schnack, D. D., Mikić, Z., & Hendrix, D. L. 1996, "Current Filaments Induced in a Resistive Corona by Continuous Footpoint Motions," *Ap. J.*, in draft.

Shibata, K. 1995, Solar Wind 8 Conference, Dana Point, CA, paper O-1-05.

Sime, D. G. 1989, *J. Geophys. Res.*, **94**, 151.

Smith, E. J., Neugebauer, M., Balogh, A., Bame, S. J., Erdos, G., Forsyth, R. J., Goldstein, B. E., Philips, J. L., & Tsurutani, B. 1993, *Geophys. Res. Lett.*, **20**, 2327.

Smith, E. J., Marsden, R. G., & Page, D. E. 1995, *Science*, **268**, 1005.

Snodgrass, H. B. 1983, *Ap.J.*, **270**, 288.

Steinolfson, R. S., Suess, S. T., & Wu, S. T. 1982, *Ap. J.*, **255**, 730.

Sturrock, P.A. 1991, *Ap. J.*, **380**, 655.

Tsuneta, S. 1996, *Ap. J.*, **456**, 840.

Vainshtein, S. I., & Parker, E. N. 1986, *Ap. J.*, **304**, 821.

van Ballegooijen, A. A. 1988, *Proc. Ninth Sacramento Peak Summer Workshop on Solar and Stellar Coronal Structure and Dynamics*, E. Altrock, ed. (Sunspot, New Mexico: National Solar Observatory) p115.

Van Hoven, G. 1981, in *Solar Flare Magnetohydrodynamics*, ed. E. R. Priest (London: Gordon & Breach), p. 217.

Van Hoven, G., & Cross, M. A. 1973, *Phys. Rev.*, **A7**, 1347.

Van Hoven, G., Mok, Y., & Mikić, Z., 1995a, *Ap. J.*, **440**, L105.

Van Hoven, G., Mok, Y., & Mikić, Z., 1995b, *EOS (Trans. AGU)*, **76**, F487.

Van Hoven, G., Hendrix, D. L., & Schnack, D.D. 1995c, *J. Geophys. Res.*, **100**, 19819.

Wang, Y. M., & Sheeley, N. R. Jr. 1992, *Ap. J.*, **392**, 310.

Wang, A. H., Wu, S. T., Suess, S. T., & Poletto, G. 1993, *Sol. Phys.*, **147**, 55.

Withbroe, G. L. 1988, *Ap. J.*, **325**, 442.

Withbroe, G. L., & Noyes, R. W. 1977, *Ann. Rev. Astron. Ap.*, **15**, 363.

APPENDIX

PUBLICATIONS SUPPORTED BY NASA SPT GRANT NAG5-2257

1. "The Generation of Solar Magnetic Activity: Photospheric Flows and Coronal Fields", *Advances in Space Research*, Vol. 13, No. 9, pp. 15-22 (1993); G. Van Hoven, D. D. Schnack, Z. Mikić and J. A. Linker.
2. "Formation, Levitation and Stability of Prominences in the Magnetized Solar Atmosphere", *Ap. J.* **413**, 416 (1993); J. F. Drake, Y. Mok and G. Van Hoven.
3. "The Differential Emission Measure of Nested Hot and Cool Magnetic Loops", *Solar Phys. (Letts)* **147**, 199 (1993), G. Van Hoven and Y. Mok.
4. "Thickness Variations along Coronal Loops Inferred from Vector Magnetograph Data", *Ap. J.*, **422**, 899 (1994); A. N. McClymont and Z. Mikić.
5. "Disruption of Coronal Magnetic Field Arcades", *Ap. J.*, **430**, 898 (1994); Z. Mikić and J. A. Linker.
6. "Deducing Coronal Magnetic Fields from Vector Magnetograms", in *Solar Active Region Evolution: Comparing Models with Observations* (K. S. Balasubramaniam and G. W. Simon, eds.), Astron. Soc. Pac. Conf. Series **68**, 225 (1994); Z. Mikić and A. N. McClymont.
7. "Current Filaments Induced in a Resistive Corona by Continuous Footpoint Motions", in *Solar Active Region Evolution: Comparing Models with Observations* (K. S. Balasubramaniam and G. W. Simon, eds.), Astron. Soc. Pac. Conf. Series **68**, 180 (1994); D. D. Schnack and Z. Mikić.
8. "The Generation of Solar Magnetic Activity", in *Solar Active Region Evolution: Comparing Models with Observations* (K. S. Balasubramaniam and G. W. Simon, eds.), Astron. Soc. Pac. Conf. Series **68** , 211 (1994); G. Van Hoven, D. D. Schnack, Z. Mikić and J. A. Linker.
9. "Evolution and Disruption of Magnetic Arcades", in *Solar Active Region Evolution: Comparing Models with Observations* (K. S. Balasubramaniam and G. W. Simon, eds.), Astron. Soc. Pac. Conf. Series **68** , 251 (1994); J. A. Linker and Z. Mikić.
10. "Modeling Coronal Evolution", in *Proc. Third SOHO Workshop –Solar Dynamic Phenomena and Solar Wind Consequences*, Estes Park, Colorado, USA, p. 249 (ESA SP-373, December 1994); J. A. Linker, Z. Mikić, and D. D. Schnack.
11. "Disruption of a Helmet Streamer by Photospheric Shear", *Ap. J. Lett.* **438**, L45 (1995); J. A. Linker and Z. Mikić.
12. "Interstellar Clouds in High Speed, Supersonic Flows: Two Dimensional Simulations", *Ap. J.* **439**, 237 (1995); A. V. R. Schiano, W.A. Christiansen, and J. M. Knerr.

13. "The Solar-Surface Boundary Conditions of Coronal Magnetic Loops", *Solar Phys.*, **161**, 67 (1995); Y. Mok and G. Van Hoven.
14. "Coronal Loop Formation from Photospheric Convection", *Ap. J. Letts*, **440**, L105 (1995); G. Van Hoven, Y. Mok, and Z. Mikić.
15. "The Diagnosis of General Magnetic Reconnection", *J. Geophys. Res.*, **100**, 19819 (1995); G. Van Hoven, D. L. Hendrix and D. D. Schnack.
16. "The Evolution, Structure and Dynamics of the Magnetized Solar Corona", *Gather/Scatter* (San Diego Supercomputer Center), Vol. 11, pp 6-8 (1995); G. Van Hoven, J. A. Linker, and Z. Mikić.
17. "Modeling of Active-Region Magnetic Fields," in *Solar Drivers of Interplanetary and Terrestrial Disturbances* (K.S. Balasubramaniam, S.L. Keil, and R.N. Smartt, eds.), Astronomical Society of the Pacific, Conference Series, Vol. **95**, p. 108 (1996); Z. Mikić, J.A. Linker, and D.D. Schnack.
18. "Global Coronal Modeling and Space Weather Prediction," in *Solar Drivers of Interplanetary and Terrestrial Disturbances* (K.S. Balasubramaniam, S.L. Keil, and R.N. Smartt, eds.), Astronomical Society of the Pacific, Conference Series, Vol. **95**, p. 208 (1996); J. A. Linker, Z. Mikić, and D. D. Schnack.
19. "Surface Driven Evolution and Activity of Atmospheric Magnetic Structures", in *Magnetodynamic Phenomena in the Solar Atmosphere* , Proceedings of IAU Colloquium No. 153 (Y. Uchida, T. Kosugi and H. S. Hudson, eds.), Kluwer, Dordrecht, in press (1996); G. Van Hoven, Y. Mok and D. L. Hendrix.
20. "Large-Scale Structure of the Solar Corona and Inner Heliosphere", in the Proceedings of the *International Solar Wind 8 Conference* (S. Habbal, M. Neugebauer, J. Gosling and W. S. Kurth, eds.), Jet Propulsion Lab., in press (1996); Z. Mikić and J. A. Linker.
21. "A Dynamic Model of the Three-Fluid Solar Wind: Equilibrium Structures and Fluxes", in the Proceedings of the *International Solar Wind 8 Conference* (S. Habbal, M. Neugebauer, J. Gosling and W. S. Kurth, eds.), Jet Propulsion Lab., in press (1996); S. P. Ruden, A. V. R. Schiano and G. Van Hoven.
22. "Coronal Mass Ejections and the Evolution of the Large-Scale Corona", in the Proceedings of the *International Solar Wind 8 Conference* (S. Habbal, M. Neugebauer, J. Gosling and W. S. Kurth, eds.), Jet Propulsion Lab., in press (1996); J. A. Linker and Z. Mikić.
23. "Convectively Driven Magnetohydrodynamic Turbulence and Coronal Heating", *Ap. J.*, **467**, xxx (1996); D. L. Hendrix and G. Van Hoven.
24. "On the Viability of Ohmic Dissipation as a Coronal Heating Source", *Ap. J.*, **470**, xxx (1996); D. L. Hendrix, G. Van Hoven, Z. Mikić, and D. D. Schnack.
25. "Current Filaments Induced in a Resistive Corona by Continuous Footpoint Motions", *Ap. J.*, submitted (1996); D. D. Schnack, Z. Mikić and D. L. Hendrix.